Received: 3 February 2020 | Revised: 15 June 2020 | Accepted: 11 August 2020

DOI: 10.1002/ajpa.24140

BRIEF COMMUNICATION

American Journal of PHYSICAL ANTHROPOLOGY WILEY

morphomap: An R package for long bone landmarking, cortical thickness, and cross-sectional geometry mapping

Antonio Profico[1] | Luca Bondioli[2] | Pasquale Raia[3] | Paul O'Higgins[1,4,5] | Damiano Marchi[6,7]

[1]PalaeoHub, Department of Archaeology, University of York, York, UK

[2]Service of Bioarchaeology Service, Museo delle Civiltà, Rome, Italy

[3]Dipartimento di Scienze della Terra, dell'Ambiente e delle Risorse, Università di Napoli Federico II, Naples, Italy

[4]Hull York Medical School, University of York, York, UK

[5]Centre for Forensic Anthropology, University of Western Australia, Perth, Australia

[6]Department of Biology, University of Pisa, Pisa, Italy

[7]Evolutionary Studies Institute and Centre for Excellence in PalaeoSciences, University of the Witwatersrand, Johannesburg-Braamfontein, South Africa

Correspondence
Antonio Profico, PalaeoHub, Department of Archaeology, University of York, York YO10 5DD, UK.
Email: antonio.profico@york.ac.uk

Funding information
H2020 Marie Skłodowska-Curie Actions, Grant/Award Number: 835571

Abstract

Objectives: This study describes and demonstrates the functionalities and application of a new R package, *morphomap*, designed to extract shape information as semi-landmarks in multiple sections, build cortical thickness maps, and calculate biomechanical parameters on long bones.

Methods: *morphomap* creates, from a single input (an oriented 3D mesh representing the long bone surface), multiple evenly spaced virtual sections. *morphomap* then directly and rapidly computes morphometric and biomechanical parameters on each of these sections. The R package comprises three modules: (a) to place semilandmarks on the inner and outer outlines of each section, (b) to extract cortical thicknesses for 2D and 3D morphometric mapping, and (c) to compute cross-sectional geometry.

Results: In this article, we apply *morphomap* to femora from *Homo sapiens* and *Pan troglodytes* to demonstrate its utility and show its typical outputs. *morphomap* greatly facilitates rapid analysis and functional interpretation of long bone form and should prove a valuable addition to the osteoarcheological analysis software toolkit.

Conclusions: Long bone loading history is commonly retrodicted by calculating biomechanical parameters such as area moments of inertia, analyzing external shape and measuring cortical thickness. *morphomap* is a software written in the open source R environment, it integrates the main methodological approaches (geometric morphometrics, cortical morphometric maps, and cross-sectional geometry) used to parametrize long bones.

KEYWORDS

cross-sectional geometry, geometric morphometrics, long bones, morphomap, morphometric maps, R

1 | INTRODUCTION

The study of diaphyseal bone form based on landmarks or measurements between them, cortical thickness variations and cross-sectional geometry (CSG) are commonly carried to retrodict long bone behavior and adaptation in response to loading. Such analyses are applicable in studies of the impacts on adult form and developing bones of locomotion, the nature, intensity and repetitiveness of physical activity and

body mass. In the field of specialism of the authors, biological anthropology, many past studies have used parameters of form, cortical thicknesses or CSG, to study past behavior and loading, in primates (Connour, Glander, & Vincent, 2000; Kimura, 2003; Marchi, 2005, 2007, 2010; Marchi, Leischner, Pastor, & Hartstone-Rose, 2018; Patel, Ruff, Simons, & Organ, 2013; Ruff, 2002; Ruff & Runestad, 1992), ancient human populations (Carlson & Marchi, 2014; Holt, 2003; Macintosh, Davies, Pinhasi, & Stock, 2015; Macintosh, Pinhasi, & Stock, 2017; Marchi, Sparacello, Holt, & Formicola, 2006; Niinimäki et al., 2017; Ruff & Hayes, 1983; Ruff & Larsen, 2014; Shaw & Stock, 2013; Sparacello, Marchi, & Shaw, 2014; Stock & Pfeiffer, 2001), and fossil hominins (Friedl et al., 2019; Jungers & Minns, 1979; Marchi, Harper, Chirchir, & Ruff, 2019; Rodríguez, Carretero, García-González, & Arsuaga, 2018; Ruff, Burgess, Ketcham, & Kappelman, 2016; Ruff, Trinkaus, Walker, & Larsen, 1993; Trinkaus & Ruff, 1989, 2012). While parameters describing bone form, cortical thickness variations and CSG have proven to be very useful for reconstructing bone loading patterns (Endo & Takahashi, 1982; Huiskes, 1982; Piziali, Hight, & Nagel, 1976; Uhthoff & Jaworski, 1978), the effort in calculation has tended to limit studies to a few cross-sections, although some previous studies have shown the value of finer detailed analysis of whole long bone shafts and multiple sections (Lacoste Jeanson, Santos, Dupej, 2018; Lacoste Jeanson, Santos, Villa, et al., 2018; Puymerail et al., 2012).

Computerized tomography (CT) scanning and advances in three dimensional (3D) reconstruction, visualization, parameterization, and analysis of skeletal form have facilitated the collection, sharing (i.e., morphosource, MorphoMuseum, Digital Morphology museum available at http://dmm.pri.kyoto-u.ac.jp, Kupri and NESPOS) (Boyer, Gunnell, Kaufman, & McGeary, 2016; Bradtmöller, Pastoors, Slizewski, & Weniger, 2010; Lebrun & Orliac, 2016) interpretation of large datasets (Davies et al., 2017). These advances underpin a specific subdiscipline within our field of biological anthropology, virtual anthropology (VA; Weber, Recheis, Scholze, & Seidler, 1998; Weber, 2001; Cunningham, Rahman, Lautenschlager, Rayfield, & Donoghue, 2014). The methods of VA are applicable to skeletal studies in all species.

Increasingly, studies utilize skeletal landmark coordinates to investigate form variation using geometric morphometric (GM) methods. However, while landmarks can readily be identified in the cranium (Cardini & O'Higgins, 2004; Mitteroecker, Gunz, & Bookstein, 2005) and epiphyses (Almécija et al., 2019; Arias-Martorell, Potau, Bello-Hellegouarch, Pastor, & Pérez-Pérez, 2012; Brzobohatá, Krajíček, Velemínský, Poláček, & Velemínská, 2014; Galletta, Stephens, Bardo, Kivell, & Marchi, 2019; Harmon, 2007; Holliday, Hutchinson, Morrow, & Livesay, 2010; Rein, 2019), the diaphysis presents fewer unequivocal matching points between specimens. Therefore, semilandmarks (landmarks placed according to some mathematical rule, e.g., evenly spaced around an outline) offer a potential solution, to characterize both external and internal diaphyseal surface form, albeit with limitations and complications (Brzobohatá et al., 2014; Cardini, O'Higgins, & Rohlf, 2019; De Groote, Lockwood, & Aiello, 2010; Frelat, Katina, Weber, & Bookstein, 2012; Gunz, Mitteroecker, & Bookstein, 2005; Morimoto, De León, & Zollikofer, 2011; Morimoto, Nakatsukasa, de León, & Zollikofer, 2018; Oxnard & O'Higgins, 2009).

One of the most recent developments of VA in functional morphology is the creation of morphometric maps (MMs) aimed at visualizing bone thickness variations along the diaphysis. MMs were first introduced by Amtmann and Schmitt (1968) for visualization in two dimensions (2D). The method was first taken up in medical studies (Benson, Prihoda, & Glass, 1991; Garn, Poznanski, & Nagy, 1971; Poole et al., 2012; Treece, Poole, & Gee, 2012) and only later were MM formalized as color maps and combined with 3D imaging for applications in comparative studies of cortical thickness variation in relation to locomotion (Bondioli et al., 2010; Jashashvili, Dowdeswell, Lebrun, & Carlson, 2015; Puymerail et al., 2012; Puymerail & O'Higgins, 2013; Zollikofer & Ponce de León, 2001). As well as quantitative analyses of diaphyseal cortical thicknesses, MMs allow rapid visual comparison of these among individuals (Lacoste Jeanson, Santos, Dupej, 2018; Lacoste Jeanson, Santos, Villa, et al., 2018).

While landmarks and MMs measure the form of the diaphysis, CSG predicts resistance to particular loading scenarios (e.g., compression, bending, etc.) and has proven effective in retrodicting bone loading history (Endo & Takahashi, 1982; Huiskes, 1982; Piziali et al., 1976; Uhthoff & Jaworski, 1978). Analyses of CSG have been widely applied to studies of locomotion, handedness, body mass, and other aspects of habitual loading.

Here, we present *morphomap*, an R package specifically designed to extract cross-sections from long bone meshes at specified intervals along the diaphysis and to site semilandmarks on the periosteal and endosteal outlines of each cross-section and to calculate 2D and 3D MM and CSG parameters. We demonstrate the validity of this computational tool by showing that it obtains the same results as those from manual and other computational approaches. We then demonstrate the functionality of *morphomap* in comparing a human and a chimpanzee femur. The R code and examples are freely distributed in the R-package *morphomap* (Profico, Bondioli, Raia, O'Higgins, & Marchi, 2019). An R vignette with runnable examples is reported in Supporting Information.

2 | MATERIALS AND METHODS

We tested the functionality of the *morphomap* R package on a human and a chimpanzee femur. The human femur (OdN 244) is from a Northern Italian Bronze Age necropolis of Olmo di Nogara (Canci, Tafuri, Fornaciari, Cupito, & Salzani, 2011). It was imaged at the hospital of the University of Pisa using a GE LightSpeed RT16 medical CT scanner (slice thickness 0.625 mm. slice increment 0.625 mm, voltage 120 kV, X-ray tube current 300 mA, standard reconstruction algorithm, pixel size 479 μm). The chimpanzee femur (Kupri 1022) was obtained from the Digital Morphology Museum, KUPRI (http://dmm.pri.kyoto-u.ac.jp/dmm/WebGallery/index.html). Its acquisition was performed on a Toshiba Asteio medical CT scanner (slice thickness 1.0 mm, slice increment 0.4 mm, voltage 120 kV, X-ray tube current 150 mA, standard reconstruction algorithm, pixel size 399 μm). The external and internal surfaces extracted from these are included in the *morphomap* R package.

2.1 | The morphomap R package

morphomap is designed to produce by default 61 cross-sections along the diaphysis of the long bone defined at increments of 1% between 20 and 80% of its biomechanical length as it is commonly defined in studies of diaphyseal CSG (Ruff, 2002; Marchi, 2005, 2007; Figure 1a). If required, the number of sections can be changed by the user.

To extract morphometric parameters, the centroid of each cross section is first identified and its coordinates C*x* and C*y* reported. Next, a set of lines are drawn at equally spaced angles from the centroid of the section. For each line, cortical thickness is calculated as the segment length of the line intersecting the cross-section at the medullary and at the subperiosteal contours. *morphomap* can output the mean cortical thickness (MeanThick), the minimum cortical thickness (MinThick), the standard deviation of the cortical thickness (SdThick), and the maximum cortical thickness (MaxThick). Alternative calculations of thickness can also be derived with *morphomap* (e.g., between points on the medullary outline and their nearest points on the cortex). The coordinates of the points of intersection (semilandmarks) are provided as output for morphometric analysis (Figure 1b,c).

At each cross-section, *morphomap* also calculates the periosteal (ExtP, mm) and endosteal perimeters (MedP), the cortical thickness measured at the four anatomical quadrants (anterior, posterior, medial, and lateral, in mm) and the CSG variables: the total area (TotA, mm^2), the medullary area (MedA, mm^2), the cortical area (CA, mm^2), the area moments of inertia around the *y* and *x* axis, (I_x and I_y, mm^4), the maximum and minimum area moments of inertia (I_{max} and I_{min}, mm^4), the angle between the major axis and the mediolateral axis of the cross-section, theta (θ, radians), the polar moment of inertia (J, mm^4), the section moduli (Z_x,Z_y, Z_{max}, Z_{min}, and Z_{pol}, mm^4) and the maximum chord lengths from *y* and *x* axes (d^x and d_y, mm; see Supporting Information). Table 1 summarizes the main functions of *morphomap*. The *morphomap* R package is available for all major platforms (Windows, Linux/Unix and Mac OS X).

2.2 | Automatic segmentation of long bone meshes

morphomap requires an oriented long bone mesh as the input (Figure S1). The orientation of the mesh can be checked using the function *morphomapCheck* which is described in Supporting Information. It may be necessary to mirror long bones to avoid issues of laterality. This can be achieved using the *morphomapMirror* function (Table 1). The first step of the measurement procedure is the automatic separation of the periosteal and endosteal surfaces (Figure 2) by applying the CA-LSE R-tool (Computer Assisted Laser Scanner Emulator; Profico, Schlager, et al., 2018). This is carried out by the function *morphomapSegm* (Table 1).

2.3 | Extraction of cross-sections

Sectioning is carried out using the *morphomapCore* function. First, the user specifies the biomechanical length of the long mesh. Next, *morphomap* extracts by default cross-sections at regular increments of 1% (but the user can choose a different increment) along the shaft between 20 (distal) and 80% (proximal) of the biomechanical length of the bone. The user can choose to change the start and end points by defining these parameters in the function *morphomapCore*. At each level, a transverse plane (perpendicular to the frontal plane) is drawn and the intersection between the transverse plane and the two meshes (periosteal and endosteal) (Figure 2) is used to define the periosteal and endosteal outlines of each cross-section (Figure 1c).

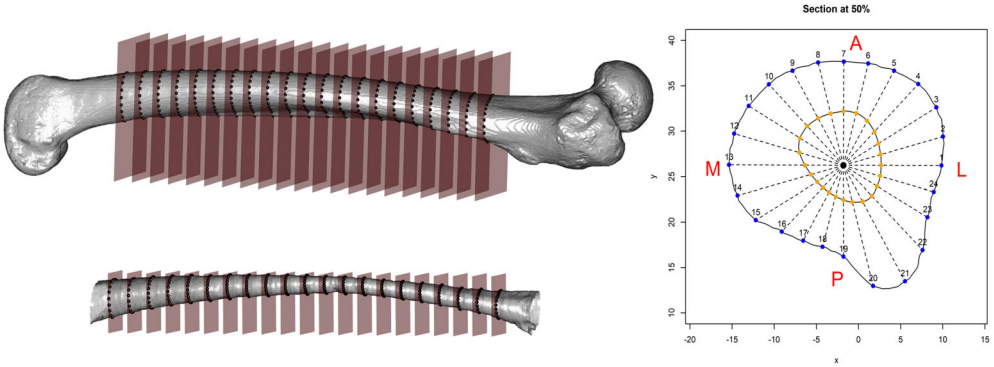

FIGURE 1 (a) Periosteal surface with 21 planes used to obtain the cross-sections; the 24 semilandmarks corresponding to the periosteal contours are reported in blue. (b) Endosteal surface with the 21 planes used to obtain the cross-sections; the 24 semilandmarks corresponding to the endosteal contours are reported in orange. (c) A cross-section at 50% of the bone biomechanical length is shown. Twenty-four lines are drawn at equally spaced angles from the centroid of the cross-section (L, lateral; A, anterior; M, medial, and P, posterior). At each angle, thickness is calculated as the segment length of the intersection of the line with the medullary and subperiosteal contours, and the points of intersection are provided as semilandmarks. In blue are shown the semilandmarks defining the periosteal contour; in orange, the semilandmarks defining the endosteal contour; the centroid of the cross-section is in black

TABLE 1 Description of the main functions of the *morphomap* R package

Function	Description	Notes
morphomapCheck	Check the orientation of the input mesh	Useful to visualize orientation of the mesh axes
morphomapMirror	Mirror a long bone mesh along the *yz* plane	Useful tool to mirror a long bone, for example, from right to left.
morphomapSegm	Separates a mesh from its visible and not visible components by using CA-LSE method	Creates the periosteal and endosteal long bone meshes
morphomapCore	Tool to slice long bones. The function creates 2D and 3D sections	The core of the *morphomap* R package. Slices the long bone and extracts cross sections
morphomapShape	Calculates equiangular semilandmarks on each cross section outline. For each cross section it extracts the coordinates of both periosteal and endosteal outlines.	Tool for extracting semilandmarks for morphometric analyses.
morphomapWriteMorphologika	Saves the semilandmark configuration in the morphologika format file	Function to export semilandmarks
morphomapPlotShape	Creates 2D and 3D plots of the semilandmark configuration	Useful to visualize the semilandmark configuration
morphomap2Dmap	Creates and plots a 2D cortical thickness map	Tool for the definition of the 2D cortical thickness map
morphomap3Dmap	Creates and plots a 3D cortical thickness map	Plots the cortical thickness dataset on the long bone mesh
morphomapPic	Saves pictures of the sections with a scale and A, L, P, and M thicknesses.	Function to export cross section
morphomapRaster	Convert a section to a raster image	Useful tool to export a cross-section of actual size
morphomapCSG	Calculates for each section the biomechanical parameters commonly used in studies of cross-sectional geometry	Tool for the calculation of the main parameters used in cross-sectional geometry studies

FIGURE 2 The output of the automatic segmentation procedure using the CA-LSE method. The method is part of the Arothron R package (Profico et al., 2018; Profico, Veneziano, Melchionna, Marchi, & Raia, 2018). The periosteal surface is shown in light green, the endosteal surface in purple

2.4 | Shape data module: Semilandmarking of cross-sections

By default, a set of 24 equiangular semilandmark pairs is defined by the intersections of the lines originating from the centroid of the cross-section and the endosteal and periosteal contours (Figure 1c). The *morphomapShape* function is used to output 2D and 3D coordinates of these semilandmarks. For subsequent analyses, the semilandmarks are numbered starting from the most anterior point on both contours, incrementing anticlockwise. The semilandmark configurations can be exported from *morphomap* in the morphologika format file (O'Higgins & Jones, 1998) using the function *morphomapWriteMorphologika*.

2.5 | MM module: Drawing of two- and three-dimensional MMs

MMs of cortical thickness facilitate visualization of the distribution of cortical bone in long bone diaphyses. They are calculated by the functions *morphomap2Dmap* and *morphomap3Dmap* from the Euclidean distances between each pair of semilandmarks (cortical and the equivalent endosteal one), which is the cortical thickness at each angle. This calculation is carried out between each pair (cortical-endosteal) of semilandmarks in each and every section. In this way, a matrix (by default, 24 distances by 61 slices) of cortical thicknesses is created, which is then converted into 2D and 3D MMs (Figure 3). 2D MMs can be drawn without any interpolation or more smoothly by applying generalized additive modeling (GAM, see Bondioli et al., 2010). 3D MMs are created by allocating to each node of the mesh the weighted (by distance) thickness values associated with its five nearest

semilandmarks (this parameter can be changed by the user). The resolution of the 2D and 3D MMs is fully customizable by the user in order to remove outliers, smooth, and scale the matrix of thickness values.

In functions *morphomap2Dmap* or *morphomap3Dmap* (Table 1) the cortical thicknesses are used to draw topographic maps in 2D or 3D. In these, colors represent thickness, standardized by default (but selectable) from 0 (minimum) to 1 (maximum), on a 100-step color (the color palette is fully customizable by the user) scale from dark red (thickest) to dark blue (thinnest). These colors are plotted in 2D with the *x* axis corresponding to the unfolded cylinder projection of the diaphysis starting and ending at the anterior (A) border passing through the lateral (L), posterior (P), and medial (M) borders. On the *y* axis is plotted the diaphyseal length expressed as a percentage of the biomechanical length (Figure 3). In 3D, a plot is returned showing the femur in four anatomical views: anterior, lateral, medial, and posterior (Figure 4).

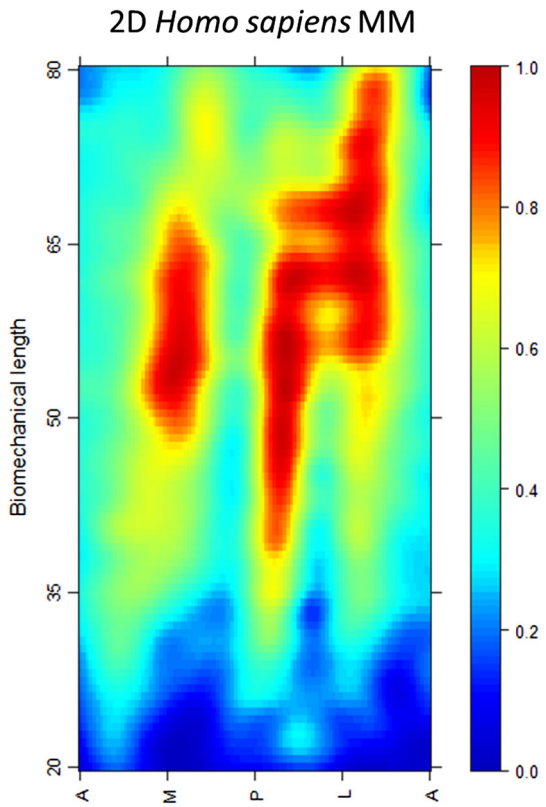

FIGURE 3 2D morphometric maps of cortical thickness along the diaphysis of OdN 244. *X* axis: unfolded cylinder projection starting and ending at the anterior (A) border, passing through the lateral (L), posterior (P), and medial (M) borders. *Y* axis: diaphyseal length expressed as a percentage of the biomechanical length from distal (bottom) to proximal (top). The colors indicate the standardized cortical thickness and range from dark red (thickest) to dark blue (thinnest)

2.6 | Exporting images of cross-sections

The *morphomapPic function* (Table 1) exports pictures of each cross-section in TIFF image format. By default, the cortical area is represented in black, the medullary canal in white. A scale bar is drawn to the bottom left (Figure 5). Thickness values at the four quadrants (A, L, P, and M) can be added to the exported cross-section (Figure 5a). The background, the legend and the cortical bone colors are fully customizable by the user.

The *morphomapRaster* function (Table 1) allows the pixel/mm ratio to be adjusted (0.1 by default) and exports the resulting bitmap (raster image) in TIFF format. This is useful to prepare images without a scale bar for importing into other morphometric or reconstruction software.

2.7 | Cross-sectional geometry module and its validation

The *morphomapCSG* function calculates in each section the CSG parameters most commonly used in biomechanical studies: the area, the area moments of inertia (I_x, I_y; Figure S4), the principal area moments of inertia (I_{max} and I_{min}; Figure S5), theta (θ), the polar moment of inertia (J) (Figure S6), and the section moduli (Z_x, Z_y, Z_{max}, Z_{min}, and Z_{pol}). The formulae used to calculate each CSG parameter implemented in *morphomap* are given in Table S1. For the calculation of these parameters *morphomap* converts the cortical area defined by periosteal and endosteal contours into picture elements of adjustable side length (delta) (Figure S2). In this way, all the parameters are calculated without interpolation. By default, delta has length 0.1 mm, this is customizable by the user (Figure S3).

We tested the calculation of CSG parameters embedded in *morphomap* by extracting two cross-sections from two surfaces artificially created for this purpose; a hollow circular cross-section and a hollow rectangular cross-section (Figure 6a,b). Table 2 shows the comparison between the values obtained via *morphomap* and those obtained by applying the formulae reported in Supporting Information.

In addition, we compared the values calculated in *morphomap* with the corresponding figures obtained when using BoneJ (Doube et al., 2010) for diaphyseal cross-sections at 50% of the total biomechanical length of a human femur (OdN 244) and a *Pan troglodytes* (Kupri 1022) femur (Figure 6). Table 3 shows the parameters calculated via *morphomap* and BoneJ.

3 | RESULTS

3.1 | Case study—The human and chimpanzee femora

In this section, we show the application of the main functions embedded in the *morphomap* R functions to a human and a chimpanzee

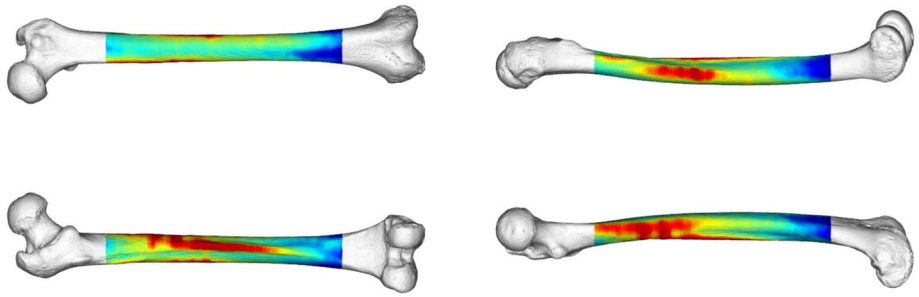

FIGURE 4 3D morphometric map of cortical thickness along the diaphysis of OdN 244. The map is shown in anterior (top left), lateral (top right), medial (bottom right) and posterior (bottom left) views. The colors indicate the standardized cortical thickness associated with each vertex of the mesh and range from dark red (thickest) to dark blue (thinnest)

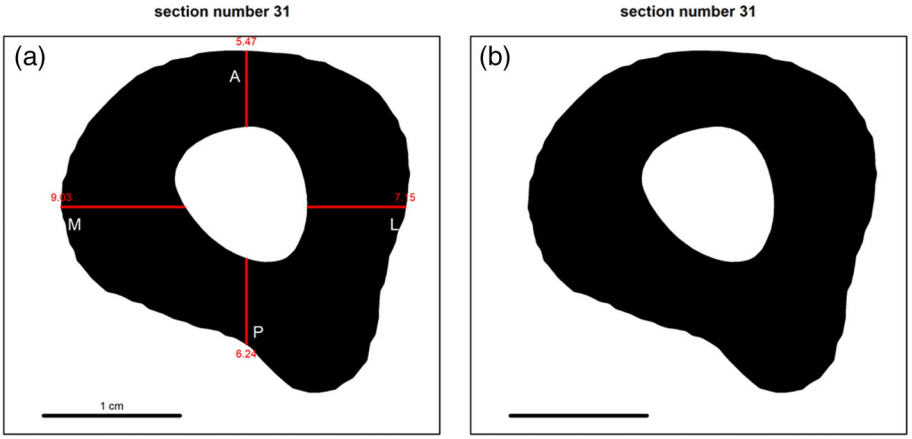

FIGURE 5 Example images of cross-sections exported from *morphomap*. (a) cross-section with anterior, lateral, posterior and medial thicknesses indicated (A, L, P, and M). (b) cross-section with no mark-up, (suitable for import into other software as BoneJ); The bar at the bottom left of each figure is the scale

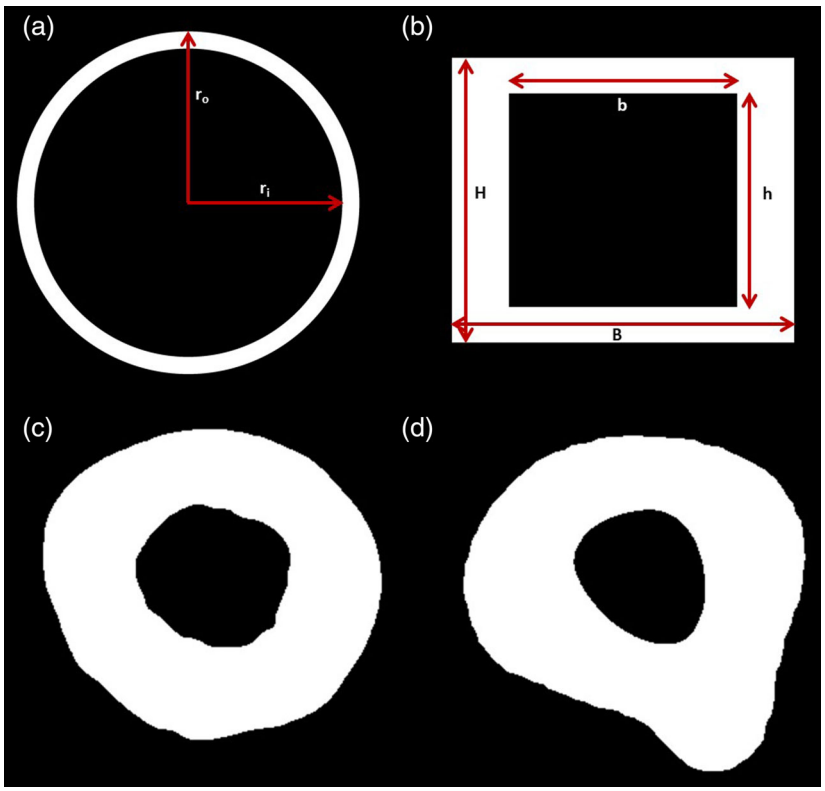

FIGURE 6 Cross-sections used to test the performance of *morphomap*. The parametric cross-sections consist of a hollow circular section (a) (r_o = 10 mm, r_i = 9 mm) and a hollow rectangular cross-section (b) (B = 24 mm, H = 20 mm, b = 16 mm, h = 15 mm). In (c) and (d) two cross-sections extracted at 50% of the biomechanical length of the femur of a chimpanzee (Kupri No. 1022) and a human (OdN 244), respectively, are represented. The pictures were exported using the function *morphomapRaster*

TABLE 2 Cross-sectional geometry of the sections in Figure 6a,b

	Geometric shapes formulae	Morphomap	Difference (%)	BoneJ	Difference (%)
	Hollow cylindric section				
I_x (mm^4)	2,700.984	2,700.602	0.01	2,706.6305	−0.21
I_y (mm^4)	2,700.984	2,700.602	0.01	2,706.6305	−0.21
CA (mm^2)	59.690	59.690	0.00	59.80	−0.18
	Hollow rectangular section				
I_x (mm^4)	11,500.00	11,500.00	0.00	11,500.00	0.00
I_y (mm^4)	17,920.00	17,920.00	0.00	17,919.8	0.00
CA (mm^2)	240.00	240.00	0.00	240.00	0.00

Note: Parameters are calculated with *morphomap* and directly using the formulae reported in Supporting Information.

TABLE 3 Cross-sectional geometric parameters calculated using *morphomap* and BoneJ on cross sections extracted at the 50% of the biomechanical length of the femur of a human (OdN 244) and of a chimpanzee (Kupri No. 1022)

	Homo sapiens			*Pan troglodytes*		
	Morphomap	BoneJ	Diff (%)	Morphomap	BoneJ	Diff (%)
Cortical area (mm^2)	386.06	386.17	−0.03	357.00	357.06	−0.02
I_x (mm^4)	15,788.98	15,795.66	−0.04	14,093.96	14,109.6	−0.11
I_y (mm^4)	18,443.6	18,444.83	−0.01	16,881.29	16,907.60	−0.16
Z_x (mm^3)	1,164.53	1,173.55	−0.77	1,203.09	1,213.32	−0.84
Z_y (mm^3)	1,358.84	1,366.66	−0.57	1,337.16	1,342.81	−0.42
I_{max} (mm^4)	19,525.64	19,540.94	−0.08	17,201.32	17,216.36	−0.09
I_{min} (mm^4)	14,668.7	14,699.94	−0.21	13,794.83	13,800.50	−0.04
Z_{max} (mm^3)	1,484.86	1,488.25	−0.23	1,312.725	1,315.87	−0.24
Z_{min} (mm^3)	1,208.47	1,213.25	−0.39	1,189.54	1,192.35	−0.24
Theta (rad)	0.50	0.50	0.00	0.31	0.31	0.00

Note: Differences in results are expressed as percentages.

femur. The detailed functionality of the R code is reported in Supporting Information. The 3D femur meshes were aligned using Avizo 6.3 (Visualization Sciences Group, Mérignac, France) following the protocol explained in Ruff (2002). The biomechanical lengths of the bones are 380.23 mm and 277.13 mm for the human and the chimpanzee, respectively. First, the mesh was uploaded into R by using the *file2mesh* function belonging to the Morpho R package (Schlager, 2017). Second, the *morphomapSegm* function was used to separate the periosteal and endosteal contours. The *morphomapSegm* function was used to produce two suitable surfaces for the extraction of the cross-sections. The *morphomapCore* function extracted sixty-one cross-sections from 20 to 80% of the biomechanical length of the two femora (see Figure 1a,b and Figures S7–S8).

Third, the *morphomapShape* function was used to extract from each cross-section 24 equiangular semi-landmarks on the periosteal and endosteal outlines (see Figure 1c). Fourth, the *morphomap2Dmap* function was used to create 2D MMs (Figure S9) and fifth, the *morphomap3Dmap* function was used to create 3D MMs (Figure 7).

In agreement with a previous study (Puymerail, 2013) performed on a sample of 12 modern humans and 10 chimpanzees, the human diaphysis shows greater cortical thickness, resisting posterior bending along the linea aspera, while the chimpanzee femur is characterized by medial and lateral bony reinforcements in the proximal portion of the bone. We have reported in Tables S2 and S3 the CSG parameters computed for the human and chimpanzee femora, respectively. These were calculated for 13 cross-sections taken a at 5% increments (for simplicity) from 20 to 80% of the biomechanical length of the femur.

Finally, *morphomap* offers the prospect of rapid processing of large samples. Table 4 shows the CPU time required to process the chimpanzee femur.

4 | DISCUSSION

Cortical bone topographic thickness variation in long bones reflects biomechanical loading history (Kivell, Davenport, Hublin, Thackeray, &

Skinner, 2018; Niinimäki et al., 2017; Ruff, Holt, & Trinkaus, 2006; Shaw & Stock, 2009). The R package, *morphomap* is intended to facilitate the work of functional morphologists in understanding how cortical bone distribution relates to loading history or other factors.

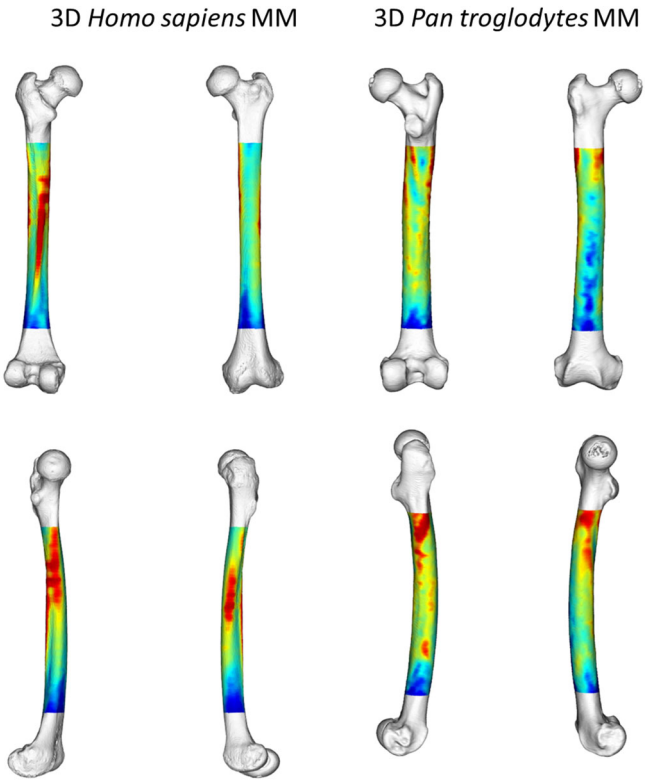

FIGURE 7 Three dimensional morphometric maps calculated on a human (OdN 244) (left) and a chimpanzee (Kupri 1022) (right) femur

Morphomap is designed to semi-automatically: (a) place semilandmarks on the inner and outer outlines of each section, (b) extract cortical thicknesses for 2D and 3D morphometric mapping, and (c) to compute cross-sectional geometry.

In this article, we detail the algorithms and tools incorporated in *morphomap* and show that its calculations are valid. The tests performed concerning the use of *morphomap* to calculate cross-sectional geometric properties are in agreement with both theoretical expectations and the results obtained using the most popular software for such purpose (i.e., BoneJ) (Doube et al., 2010). Further, we compare 2D and 3D MMs from human and chimpanzee femora and show they are in agreement with those from previous work on larger samples (Puymerail, 2013).

Thus, *morphomap* is a new tool for the study of cortical variation in long bones. It is written in the open source R environment (R Development Core Team, 2016) and is compatible with other R packages commonly used in mesh manipulation, such as Morpho (Schlager, 2017) and Arothron (Profico, Schlager, et al., 2018), morphological studies (Adams & Otárola-Castillo, 2013) and MMs (Adler, Nenadic, & Zucchini, 2003; Sarkar, 2008). *morphomap* semi-automatically processes the entire bone, beginning with an input mesh that is separated into outer and inner cortical meshes using the CAL-SE method from the Arothron R package (Profico, Veneziano, et al., 2018). The R programming language allows for easy editing of the R code for alternative implementations and debugging. The developmental version of the *morphomap* R package is available on github (https:// https://github.com/AProfico/morphomap) and the stable version is available on CRAN (https://CRAN.R-project.org/package=morphomap). We strongly encourage R developers to propose and code new functionalities to be included in *morphomap*.

TABLE 4 Details on the computation times required by *morphomap* to process the chimpanzee femur. Inter(R) Core (TM) i7-7700HQ CPU 2.80 GHz RAM memory 16.0 GB

Process	Function	Time (s)	Note
Automatic segmentation	*morphomapSegm*	17.65	347,840 vertices
Cross sections definition	*morphomapCore*	39.92	61 sections and 1,000 points on each cross section
Definition of equiangular semilandmarks	*morphomapShape*	22.39	48 semilandmarks on each cross section and definition of the centroid
Creation of 2D morphometric map	*morphomapGam* *morphomap2Dmap*	5.94	Creation and plotting of the 2D morphometric map paired with the application of GAM smoothing algorithm
Creation of 3D morphometric map	*morphomap3Dmap*	7.95	Creation and plotting of the 3D morphometric map paired with the application of GAM smoothing algorithm
Calculation of cross-sectional geometry parameter on the cross section at the 50% of the biomechanical length	*morphomapCSG*	14.91	Full calculation of the cross-sectional geometry parameters. The speed of execution mainly depends on the definition of the picture elements side length (delta) (for details see Supporting Information).
Entire process		108.76	

ACKNOWLEDGEMENTS

We thank the Digital Morphology Museum (KUPRI) for providing the 3D model of the chimpanzee femur bone. This project has received funding from the European Union's Horizon 2020 research and innovation programme (H2020 Marie Skłodowska-Curie Actions) under grant agreement H2020-MSCA-IF-2018 No. 835571 to Antonio Profico and Paul O'Higgins.

AUTHOR CONTRIBUTIONS

Antonio Profico: Conceptualization; data curation; formal analysis; funding acquisition; investigation; methodology; project administration; resources; software; validation; visualization; writing-original draft; writing-review and editing. **Luca Bondioli:** Software; writing-review and editing. **Pasquale Raia:** Software; writing-review and editing. **Paul O'Higgins:** Conceptualization; funding acquisition; methodology; project administration; software; supervision; writing-original draft; writing-review and editing. **Damiano Marchi:** Conceptualization; methodology; resources; software; supervision; validation; writing-original draft; writing-review and editing.

CONFLICT OF INTEREST

The authors declare no conflict of interest.

DATA AVAILABILITY STATEMENT

The data that support the findings of this study are included in the R package morphomap. The R package is available on CRAN at https://CRAN.R-project.org/package=morphomap.

ORCID

Antonio Profico https://orcid.org/0000-0003-2884-7118
Pasquale Raia https://orcid.org/0000-0002-4593-8006
Paul O'Higgins https://orcid.org/0000-0002-9797-0809
Damiano Marchi https://orcid.org/0000-0002-6331-8783

REFERENCES

Adams, D. C., & Otárola-Castillo, E. (2013). Geomorph: An r package for the collection and analysis of geometric morphometric shape data. *Methods in Ecology and Evolution*, *4*, 393–399.

Adler D., Nenadic O., & Zucchini W. (2003). *Rgl: A r-Library for 3d Visualization With opengl*. Proceedings of the 35th Symposium of the Interface: Computing Science and Statistics, Salt Lake City. Vol. 35. Abstract retrieved from http://rgl.neoscientists.org/arc/doc/RGL_INTERFACE03.pdf.

Almécija, S., Tallman, M., Sallam, H. M., Fleagle, J. G., Hammond, A. S., & Seiffert, E. R. (2019). Early anthropoid femora reveal divergent adaptive trajectories in catarrhine hind-limb evolution. *Nature Communications*, *10*, 1–9.

Amtmann, E., & Schmitt, H. P. (1968). Über die Verteilung der Corticalisdichte im menschlichen Femurschaft und ihre Bedeutung für die Bestimmung der Knochenfestigkeit. *Zeitschrift für Anatomie Und Entwicklungsgeschichte*, *127*, 25–41.

Arias-Martorell, J., Potau, J. M., Bello-Hellegouarch, G., Pastor, J. F., & Pérez-Pérez, A. (2012). 3D geometric morphometric analysis of the proximal epiphysis of the hominoid humerus. *Journal of Anatomy*, *221*, 394–405.

Benson, B. W., Prihoda, T. J., & Glass, B. J. (1991). Variations in adult cortical bone mass as measured by a panoramic mandibular index. *Oral Surgery, Oral Medicine, Oral Pathology*, *71*, 349–356.

Bondioli, L., Bayle, P., Dean, C., Mazurier, A., Puymerail, L., Ruff, C., … Macchiarelli, R. (2010). Morphometric maps of long bone shafts and dental roots for imaging topographic thickness variation. *American Journal of Physical Anthropology*, *142*, 328–334.

Boyer D. M., Gunnell G. F., Kaufman S., & McGeary T. M. (2016). Morphosource: Archiving and sharing 3-D digital specimen data. *Paleontological Society Papers*, *22*, 157–181. http://dx.doi.org/10.1017/scs.2017.13.

Bradtmöller M, Pastoors A, Slizewski A, Weniger G-C. 2010. *NESPOS—A Digital Archive and Platform for Pleistocene Archaeology*. Proceedings of the Data Management Workshop. Vol. 90, pp. 13–18. Abstract retrieved from https://www.tr32db.uni-koeln.de/DOI/doi.php?doiID=9.

Brzobohatá, H., Krajíček, V., Velemínský, P., Poláček, L., & Velemínská, J. (2014). The shape variability of human tibial epiphyses in an early medieval great Moravian population (9th–10th century AD): A geometric morphometric assessment. *Anthropologischer Anzeiger*, *71*, 219–236.

Canci, A., Tafuri, M., Fornaciari, G., Cupito, M., & Salzani, L. (2011). Life and death in the middle bronze age. The case study of the necropolis of Olmo di Nogara, Verona (Italy). *American Journal of Physical Anthropology*, *144*, 103–107.

Cardini, A., & O'Higgins, P. (2004). Patterns of morphological evolution in Marmota (Rodentia, Sciuridae): Geometric morphometrics of the cranium in the context of marmot phylogeny, ecology and conservation. *Biological Journal of the Linnean Society*, *82*, 385–407.

Cardini, A., O'Higgins, P., & Rohlf, F. J. (2019). Seeing distinct groups where there are none: Spurious patterns from between-group PCA. *Evolutionary Biology*, *46*, 303–316.

Carlson, K. J., & Marchi, D. (2014). *Reconstructing mobility: Environmental, behavioral, and morphological determinants*. New York, NY: Springer.

Connour, J. R., Glander, K., & Vincent, F. (2000). Postcranial adaptations for leaping in primates. *Journal of Zoology*, *251*, 79–103.

Cunningham, J. A., Rahman, I. A., Lautenschlager, S., Rayfield, E. J., & Donoghue, P. C. J. (2014). A virtual world of paleontology. *Trends in Ecology & Evolution*, *29*, 347–357.

Davies, T. G., Rahman, I. A., Lautenschlager, S., Cunningham, J. A., Asher, R. J., Barrett, P. M., … Boyer, D. M. (2017). Open data and digital morphology. *Proceedings of the Royal Society*, *284*, 20170194.

De Groote, I., Lockwood, C. A., & Aiello, L. C. (2010). A new method for measuring long bone curvature using 3D landmarks and semi-landmarks. *American Association of Physics*, *141*, 658–664.

Doube, M., Kłosowski, M. M., Arganda-Carreras, I., Cordelières, F. P., Dougherty, R. P., Jackson, J. S., … Shefelbine, S. J. (2010). BoneJ: Free and extensible bone image analysis in ImageJ. *Bone*, *47*, 1076–1079.

Endo, B., & Takahashi, H. (1982). Various methods for measuring the geometrical properties of the long bone cross section with respect to mechanics. *The Anthropological Society of Nippon*, *90*, 1–16.

Frelat, M. A., Katina, S., Weber, G. W., & Bookstein, F. L. (2012). A novel geometric morphometric approach to the study of long bone shape variation. *American Journal of Physical Anthropology*, *149*, 628–638.

Friedl, L., Claxton, A. G., Walker, C. S., Churchill, S. E., Holliday, T. W., Hawks, J., … Marchi, D. (2019). Femoral neck and shaft structure in Homo Naledi from the Dinaledi chamber (rising star system, South Africa). *Journal of Human Evolution*, *133*, 61–77.

Galletta, L., Stephens, N. B., Bardo, A., Kivell, T. L., & Marchi, D. (2019). Three-dimensional geometric morphometric analysis of the first metacarpal distal articular surface in humans, great apes and fossil hominins. *Journal of Human Evolution*, *132*, 119–136.

Garn, S. M., Poznanski, A. K., & Nagy, J. M. (1971). Bone measurement in the differential diagnosis of osteopenia and osteoporosis. *Radiology*, *100*, 509–518.

Gunz, P., Mitteroecker, P., & Bookstein, F. L. (2005). Semilandmarks in three dimensions. In *Modern morphometrics in physical anthropology* (pp. 73–98). Boston, MA: Springer.

Harmon, E. H. (2007). The shape of the hominoid proximal femur: A geometric morphometric analysis. *Journal of Anatomy*, *210*, 170–185.

Holliday, T. W., Hutchinson, V. T., Morrow, M. M. B., & Livesay, G. A. (2010). Geometric morphometric analyses of hominid proximal femora: Taxonomic and phylogenetic considerations. *Homo*, *61*, 3–15.

Holt, B. M. (2003). Mobility in upper Paleolithic and Mesolithic Europe: Evidence from the lower limb. *American Journal of Physical Anthropology*, *122*, 200–215.

Huiskes, R. (1982). On the modelling of long bones in structural analyses. *Journal of Biomechanics*, *15*, 65–69.

Jashashvili, T., Dowdeswell, M. R., Lebrun, R., & Carlson, K. J. (2015). Cortical structure of hallucal metatarsals and locomotor adaptations in hominoids. *PLoS One*, *10*, e0117905.

Jungers, W. L., & Minns, R. J. (1979). Computed tomography and biomechanical analysis of fossil long bones. *American Journal of Physical Anthropology*, *50*, 285–290.

Kimura, T. (2003). Differentiation between fore-and hindlimb bones and locomotor behaviour in primates. *Folia Primatologica*, *74*, 17–32.

Kivell, T. L., Davenport, R., Hublin, J., Thackeray, J. F., & Skinner, M. M. (2018). Trabecular architecture and joint loading of the proximal humerus in extant hominoids, Ateles, and Australopithecus africanus. *American Journal of Physical Anthropology*, *167*, 348–365.

Lacoste Jeanson, A., Santos, F., Dupej, J., Velemínská, J., & Brůžek, J. (2018). Sex-specific functional adaptation of the femoral diaphysis to body composition. *American Journal of Human Biology*, *30*, e23123.

Lacoste Jeanson, A., Santos, F., Villa, C., Banner, J., & Brůžek, J. (2018). Architecture of the femoral and tibial diaphyses in relation to body mass and composition: Research from whole-body CT scans of adult humans. *American Journal of Physical Anthropology*, *167*, 813–826.

Lebrun, R., & Orliac, M. J. (2016). Morphomuseum: An online platform for publication and storage of virtual specimens. *Paleontological Society Papers*, *22*, 183–195.

Macintosh, A. A., Davies, T. G., Pinhasi, R., & Stock, J. T. (2015). Declining tibial curvature parallels∼ 6150 years of decreasing mobility in central european agriculturalists. *American Journal of Physical Anthropology*, *157*, 260–275.

Macintosh, A. A., Pinhasi, R., & Stock, J. T. (2017). Prehistoric women's manual labor exceeded that of athletes through the first 5500 years of farming in Central Europe. *Science Advances*, *3*, eaao3893.

Marchi, D. (2005). The cross-sectional geometry of the hand and foot bones of the Hominoidea and its relationship to locomotor behavior. *Journal of Human Evolution*, *49*, 743–761.

Marchi, D. (2007). Relative strength of the tibia and fibula and locomotor behavior in hominoids. *Journal of Human Evolution*, *53*, 647–655.

Marchi, D. (2010). Articular to diaphyseal proportions of human and great ape metatarsals. *American Journal of Physical Anthropology*, *143*, 198–207.

Marchi, D., Harper, C. M., Chirchir, H., & Ruff, C. B. (2019). Relative fibular strength and locomotor behavior in KNM-WT 15000 and OH 35. *Journal of Human Evolution*, *131*, 48–60.

Marchi, D., Leischner, C. L., Pastor, F., & Hartstone-Rose, A. (2018). Leg muscle architecture in primates and its correlation with locomotion patterns. *The Anatomical Record*, *301*, 515–527.

Marchi, D., Sparacello, V. S., Holt, B. M., & Formicola, V. (2006). Biomechanical approach to the reconstruction of activity patterns in Neolithic Western Liguria, Italy. *American Journal of Physical Anthropology*, *131*, 447–455.

Mitteroecker, P., Gunz, P., & Bookstein, F. L. (2005). Heterochrony and geometric morphometrics: A comparison of cranial growth in *Pan paniscus* versus *Pan troglodytes*. *Evolution & Development*, *7*, 244–258.

Morimoto, N., De León, M. S. P., & Zollikofer, C. P. E. (2011). Exploring femoral diaphyseal shape variation in wild and captive chimpanzees by means of morphometric mapping: A test of Wolff's law. *The Anatomical Record: Advances in Integrative Anatomy and Evolutionary Biology*, *294*, 589–609.

Morimoto, N., Nakatsukasa, M., de León, M. S. P., & Zollikofer, C. P. E. (2018). Femoral ontogeny in humans and great apes and its implications for their last common ancestor. *Scientific Reports*, *8*, 1930.

Niinimäki, S., Narra, N., Härkönen, L., Abe, S., Nikander, R., Hyttinen, J., … Sievänen, H. (2017). The relationship between loading history and proximal femoral diaphysis cross-sectional geometry. *American Journal of Human Biology*, *29*, e22965.

O'Higgins, P., & Jones, N. (1998). Facial growth in *Cercocebus torquatus*: An application of three-dimensional geometric morphometric techniques to the study of morphological variation. *Journal of Anatomy*, *193*, 251–272.

Oxnard, C., & O'Higgins, P. (2009). Biology clearly needs morphometrics. Does morphometrics need biology? *Biological Theory*, *4*, 84–97.

Patel, B. A., Ruff, C. B., Simons, E. L. R., & Organ, J. M. (2013). Humeral cross-sectional shape in suspensory primates and sloths. *The Anatomical Record*, *296*, 545–556.

Piziali, R. L., Hight, T. K., & Nagel, D. A. (1976). An extended structural analysis of long bones—Application to the human tibia. *Journal of Biomechanics*, *9*, 695–701.

Poole, K. E. S., Treece, G. M., Mayhew, P. M., Vaculík, J., Dungl, P., Horák, M., … Gee, A. H. (2012). Cortical thickness mapping to identify focal osteoporosis in patients with hip fracture. *PLoS One*, *7*, e38466.

Profico A, Bondioli L, Raia P, O'Higgins P, Marchi D. 2019. morphomap: morphometric maps, shape data and cross sectional geometry. R package version 1.2.

Profico, A., Schlager, S., Valoriani, V., Buzi, C., Melchionna, M., Veneziano, A., … Manzi, G. (2018). Reproducing the internal and external anatomy of fossil bones: Two new automatic digital tools. *American Journal of Physical Anthropology*, *166*, 979–986.

Profico A, Veneziano A, Melchionna M, Marchi D, Raia P. 2018. Arothron: R functions for geometric morphometrics analyses. R package version 1.1.

Puymerail, L. (2013). The functionally-related signatures characterizing the endostructural organisation of the femoral shaft in modern humans and chimpanzee. *Comptes Rendus Palevol*, *12*, 223–231.

Puymerail L, O'Higgins P. 2013. *Reading Function from Long Bones: Implications for the Reconstruction of Early Hominin Postural and Locomotor Behaviours*. 3rd Annual Meeting, European Society for the study in Human Evolution, Vienna, Austria. Abstract retrieved from https://www.eshe.eu/static/eshe/files/ESHE_Vienna_2013_Abstracts.pdf.

Puymerail, L., Ruff, C. B., Bondioli, L., Widianto, H., Trinkaus, E., & Macchiarelli, R. (2012). Structural analysis of the Kresna 11 Homo erectus femoral shaft (Sangiran, Java). *Journal of Human Evolution*, *63*, 741–749.

R Development Core Team. (2016). *R: A language and environment for statistical computing*. Vienna, Austria: R Foundation for Statistical Computing.

Rein, T. R. (2019). A geometric morphometric examination of hominoid third metacarpal shape and its implications for inferring the precursor to terrestrial bipedalism. *The Anatomical Record*, *302*, 983–998.

Rodríguez, L., Carretero, J. M., García-González, R., & Arsuaga, J. L. (2018). Cross-sectional properties of the lower limb long bones in the middle Pleistocene Sima de los Huesos sample (sierra de Atapuerca, Spain). *Journal of Human Evolution*, *117*, 1–12.

Ruff, C., Holt, B., & Trinkaus, E. (2006). Who's afraid of the big bad Wolff?: "Wolff's law" and bone functional adaptation. *American Journal of Physical Anthropology*, *129*, 484–498.

Ruff, C. B. (2002). Long bone articular and diaphyseal structure in Old World monkeys and apes. I: Locomotor effects. *American Journal of Physical Anthropology*, *119*, 305–342.

Ruff, C. B., Burgess, M. L., Ketcham, R. A., & Kappelman, J. (2016). Limb bone structural proportions and locomotor behavior in AL 288-1 ("Lucy"). *PLoS One*, *11*, e0166095.

Ruff, C. B., & Hayes, W. C. (1983). Cross-sectional geometry of Pecos Pueblo femora and tibiae—A biomechanical investigation: I. method

and general patterns of variation. *American Journal of Physical Anthropology*, *60*, 359–381.

Ruff, C. B., & Larsen, C. S. (2014). Long bone structural analyses and the reconstruction of past mobility: A historical review. In *Reconstructing mobility* (pp. 13–29). New York, NY: Springer.

Ruff, C. B., & Runestad, J. A. (1992). Primate limb bone structural adaptations. *Annual Review of Anthropology*, *21*, 407–433.

Ruff, C. B., Trinkaus, E., Walker, A., & Larsen, C. S. (1993). Postcranial robusticity in Homo. I: Temporal trends and mechanical interpretation. *American Journal of Physical Anthropology*, *91*, 21–53.

Sarkar, D. (2008). *Lattice: Multivariate data visualization with R*. Seattle, WA: Springer Science & Business Media.

Schlager, S. (2017). Chapter 9—Morpho and Rvcg – shape analysis in R: R-packages for geometric morphometrics, shape analysis and surface manipulations. In *Statistical shape and deformation analysis*. (pp. 217–256). Cambridge, UK: Academic Press.

Shaw, C. N., & Stock, J. T. (2009). Intensity, repetitiveness, and directionality of habitual adolescent mobility patterns influence the tibial diaphysis morphology of athletes. *American Journal of Physical Anthropology*, *140*, 149–159.

Shaw, C. N., & Stock, J. T. (2013). Extreme mobility in the late Pleistocene? Comparing limb biomechanics among fossil Homo, varsity athletes and Holocene foragers. *Journal of Human Evolution*, *64*, 242–249.

Sparacello, V. S., Marchi, D., & Shaw, C. N. (2014). The importance of considering fibular robusticity when inferring the mobility patterns of past populations. In *Reconstructing mobility* (pp. 91–110). New York, NY: Springer.

Stock, J., & Pfeiffer, S. (2001). Linking structural variability in long bone diaphyses to habitual behaviors: Foragers from the southern African later stone age and the Andaman Islands. *American Journal of Physical Anthropology*, *115*, 337–348.

Treece, G. M., Poole, K. E. S., & Gee, A. H. (2012). Imaging the femoral cortex: Thickness, density and mass from clinical CT. *Medical Image Analysis*, *16*, 952–965.

Trinkaus, E., & Ruff, C. B. (1989). Diaphyseal cross-sectional morphology and biomechanics of the fond-de-Forêt 1 femur and the spy 2 femur and tibia. *Bull Soc R Belge Anthropol Prehist*, *100*, 33–42.

Trinkaus, E., & Ruff, C. B. (2012). Femoral and tibial diaphyseal cross-sectional geometry in Pleistocene Homo. *PaleoAnthropology*, *2012*, 13–62.

Uhthoff, H. K., & Jaworski, Z. F. (1978). Bone loss in response to long-term immobilisation. *Journal of Bone and Joint Surgery. British Volume (London)*, *60*, 420–429.

Weber, G. W. (2001). Virtual anthropology (VA): A call forGlasnost in paleoanthropology. *The Anatomical Record*, *265*, 193–201.

Weber, G. W., Recheis, W., Scholze, T., & Seidler, H. (1998). Virtual anthropology (VA): Methodological aspects of linear and volume measurements—First results. *Collegium Antropologicum*, *22*, 575–584.

Zollikofer, C. P. E., & Ponce de León, M. S. (2001). Computer-assisted morphometry of hominoid fossils: The role of morphometric maps. In *Phylogeny of the neogene hominoid primates of eurasia* (pp. 50–59). Cambridge, UK: Cambridge University Press.

SUPPORTING INFORMATION

Additional supporting information may be found online in the Supporting Information section at the end of this article.

How to cite this article: Profico A, Bondioli L, Raia P, O'Higgins P, Marchi D. morphomap: An R package for long bone landmarking, cortical thickness, and cross-sectional geometry mapping. *Am J Phys Anthropol*. 2021;174:129–139. https://doi.org/10.1002/ajpa.24140